Nano Energy 37 (2017) 7–14

Contents lists available at ScienceDirect

Nano Energy

journal homepage: www.elsevier.com/locate/nanoen

Full paper

Multifunctional Co_3S_4@sulfur nanotubes for enhanced lithium-sulfur battery performance

Jun Pu[a], Zihan Shen[a], Jiaxin Zheng[b], Wenlu Wu[b], Chao Zhu[a], Qingwen Zhou[a], Huigang Zhang[a,*], Feng Pan[b]

[a] National Laboratory of Solid State Microstructures, College of Engineering and Applied Sciences, and Collaborative Innovation Center of Advanced Microstructures, Institute of Materials Engineering, Nanjing University, Jiangsu, PR China
[b] School of Advanced Materials, Peking University, Shenzhen Graduate School, Shenzhen, PR China

ARTICLE INFO

Keywords:
Lithium sulfur batteries
Cobalt sulfides
Nanotubes
Cathodes
Nanostructures

ABSTRACT

Lithium sulfur batteries attract the increasing attentions because of the high energy density. However, sulfur cathodes suffer from several scientific and technical issues which are related to polysulfide ion migration, low conductivity, and volume changes. Many strategies such as porous hosts, polysulfide adsorbents, catalyst, and conductive fillers and so on have been proposed to address these issues, separately. In this study, novel Co_3S_4 nanotubes are developed to efficiently host sulfur, adsorb polysulfide, and catalyze their conversion. Because of these multifunctional advantages in one structure, the resulting Co_3S_4@S nanotube electrodes demonstrate superior electrochemical properties for high performance lithium sulfur batteries.

1. Introduction

Lithium-sulfur (Li-S) batteries are receiving great attentions because of their high theoretical energy density (~2600 Wh kg^{-1}) [1,2], low cost, environmental friendliness, and natural abundance of sulfur resources [3–6]. Although Li-S batteries have many advantages, they suffer from several scientific and technical issues, which impede the practical implementation [7]. First, sulfur is an insulator with a very low conductivity of only 5×10^{-28} S m^{-1} [8], which limits the sulfur utilization and reduces the rate capability of Li-S batteries [9]. Second, the "shuttle effect" caused by polysulfides dissolution and diffusion decreases the specific capacity and Coulombic efficiency [10–15]. Third, the volume changes during sulfur lithiation/delithiation may damage the cathode structure and lower cycling performance of Li-S batteries [16].

Recently, nanostructured carbons, such as meso/micro-porous carbons [17,18], hollow carbon spheres [19,20], graphene [21–23], carbon nanotubes [24–26], and nanofibers [27,28], have been proposed to host sulfur materials. Because carbon is able to provide a rapid electron pathway and hollow structures physically trap polysulfides, the resulting carbon/sulfur composites prolong the cycle lives and increase the deliverable capacities [29]. However, carbon matrix is repellent to the polysulfides. During long-term cycling, sulfur species detach from the carbon matrix [30,31]. The weak interaction between polysulfide species and carbon matrix raises the charge transfer resistance and reduces the redox kinetics of polysulfides [32–34]. Recently, it was reported that heteroatom doped carbon provides the abundant adsorption sites and strong chemisorption of polysulfides to address the issues [35]. Ti_4O_7 [30], $NiFe_2O_4$ [36], TiO_2 [37], MnO_2 [38], Ti_nO_{2n-1} and some other metal oxides [39,40], demonstrated the strong affinity to polysulfides and the high capacity retention when used in the cathodes of Li-S batteries. However, these metal oxides usually have relatively low electronic conductivity which reduces the electrode kinetics. To explore more conductive polysulfide adsorbents, the research attentions have been turned to transition metal sulfides because some of them usually have the relatively high electronic conductivity. As the absorbent and conducting phase, the sulfides must first have high bulk conductivity to facilitate charge transports through the interfaces and electrodes. More importantly, a continuous electronic network is necessary to improve the overall electrode conductivity. Fiber or whisker-like morphology has a low percolation threshold to form a continuous conducting network. Thus, the conductive absorbents with high aspect ratios and hollow structures are highly desired for sulfur cathodes.

Since the charged and discharged products of sulfur are insoluble in the non-aqueous electrolytes and only the soluble polysulfide intermediates are mobile between cathodes and anodes, a rapid and catalytic conversion of sulfur species may have the same consequence as suppressing the shuttle effects and confining the sulfides inside cathodes by using hollow hosts. Nickel sulfide prepared by ball milling

* Corresponding author.
E-mail address: hgzhang@nju.edu.cn (H. Zhang).

http://dx.doi.org/10.1016/j.nanoen.2017.05.009
Received 10 April 2017; Received in revised form 3 May 2017; Accepted 3 May 2017
Available online 04 May 2017
2211-2855/ © 2017 Elsevier Ltd. All rights reserved.

nickel and sulfur were first found to be catalytic for Li-S redox reactions [41]. Pt, Al, Ni, metal oxides, and heteratom-doped carbon have been explored to catalyze the Li-S redox reactions [42–47]. To further enhance the conversion kinetics of redox shuttles by electrocatalysts, the polysulfide anions must at best be chemically entrapped by the functional groups of catalyst materials and physically confined by structured hosts.

Recent reports about sulfides absorbents found that cobalt sulfides (CoS_2 and Co_9S_8) have the strong affinity to sulfur species [48,49]. Especially, CoS_2 exhibits the good catalytic properties for the sulfur species conversion [48,50,51]. There are five intermediate phases ($Co_4S_{3\pm y}$, Co_9S_8, $Co_{1-y}S$, Co_3S_4, and CoS_2) in the Co-S binary systems [52]. $Co_4S_{3\pm y}$ and $Co_{1-y}S$ are stable only at high temperatures. CoS_2 (6.7×10^5 S m^{-1}) [53] and Co_3S_4 (3.3×10^5 S m^{-1}) [54] have much higher conductivity than Co_9S_8 (1.36 S m^{-1}) [55]. Earlier research reported that Co_3S_4 has 2–3 times the electrocatalytic capability of CoS_2 for oxygen reduction reactions [56]. Co_3S_4 has not been studied for catalyzing the conversion of sulfur species which is in the same group as oxygen in the periodic table. It intrigues us to tentatively explore what influences the catalytic, morphologic, and conducting properties of spinel Co_3S_4 have on Li-S batteries.

In this contribution, we developed a facile route to produce Co_3S_4@S nanotubes for high-performance Li-S batteries. As shown in Fig. 1a, the catalytic, morphologic, and conducting properties of polysulfide adsorbents/hosts are considered together to enhance the electrochemical properties of Li-S batteries. Nanostructured Co_3S_4 aims to absorb and catalyze the sulfur species by the relatively large surface area. The nanotube morphology helps to host sulfur species. The metallic conductivity of Co_3S_4 accelerates the kinetics. Due to these designs, the Co_3S_4@S nanotubes cathode is able to deliver a capacity of 1267 mA h g−1 AS (active sulfur basis) at 0.05 C. It shows a slow capacity decay rate of 0.041% per cycle through 1000 cycles, which significantly improves the electrochemical properties of Li-S batteries.

2. Experimental section

2.1. Synthesis of Co_3S_4 nanotubes

All the chemicals were purchased from Sinopharm Chemical Reagent Corporation and used without further purification. About 4 mmol of $CoCl_2{\cdot}6H_2O$ and 20 mmol of $CO(NH_2)_2$ were dissolved in 50 mL deionized water. The solution obtained was transferred to a Teflon-lined stainless-steel autoclave and heated at 95 °C for 8 h. After cooling down to room temperature, the precursor precipitates were filtered, rinsed, and dried in vacuum. The dry powder (~0.072 g) obtained was added into 1 M thioacetamide solution (40 mL). After hydrothermally treated at 200 °C for 12 h, the black precipitates in the autoclave were filtered, washed, and dried under vacuum at 50 °C for 2 h.

2.2. Synthesis of Co_3S_4 nanotubes and sulfur composite

The Co_3S_4@S nanotube composite was prepared via a simple melt-diffusion method. The mixture of sulfur and Co_3S_4 nanotubes was heated at 155 °C for 10 h in a sealed vessel. The composite electrodes with the varied mass ratios of sulfur and Co_3S_4 nanotubes were prepared and characterized for comparison.

2.3. Synthesis of Co_3S_4 nanoparticles

In a typical synthesis, 20 mmol $Co(NO_3)_2{\cdot}6H_2O$ and 6 mmol NaOH were slowly dissolved in 60 mL deionized water under stirring. After the suspension was formed, about 4 mmol thioacetamide was dissolved into the solution under vigorous stirring for 30 min. The turbid solution obtained was transferred to a Teflon-lined stainless-steel autoclave and heated at 200 °C for 12 h. After cooling down naturally to room temperature, the precipitates were filtered, washed, and dried.

2.4. Materials characterization

X-ray diffraction (XRD) patterns of all samples were collected by a Rigaku D/Max III with Cu Kα radiation. The morphology observation was conducted within a Zeiss Ultra 55 field-emission scanning electron microscope (SEM). X-ray photoelectron spectra (XPS) were recorded on an ESCALab MKII X-ray photoelectron spectrometer with Mg Kα X-ray as the excitation source. The binding energies in XPS analysis were calibrated by C 1 s at 284.6 eV. Transmission electron microscope (TEM), high-resolution TEM (HRTEM) images, and energy dispersive

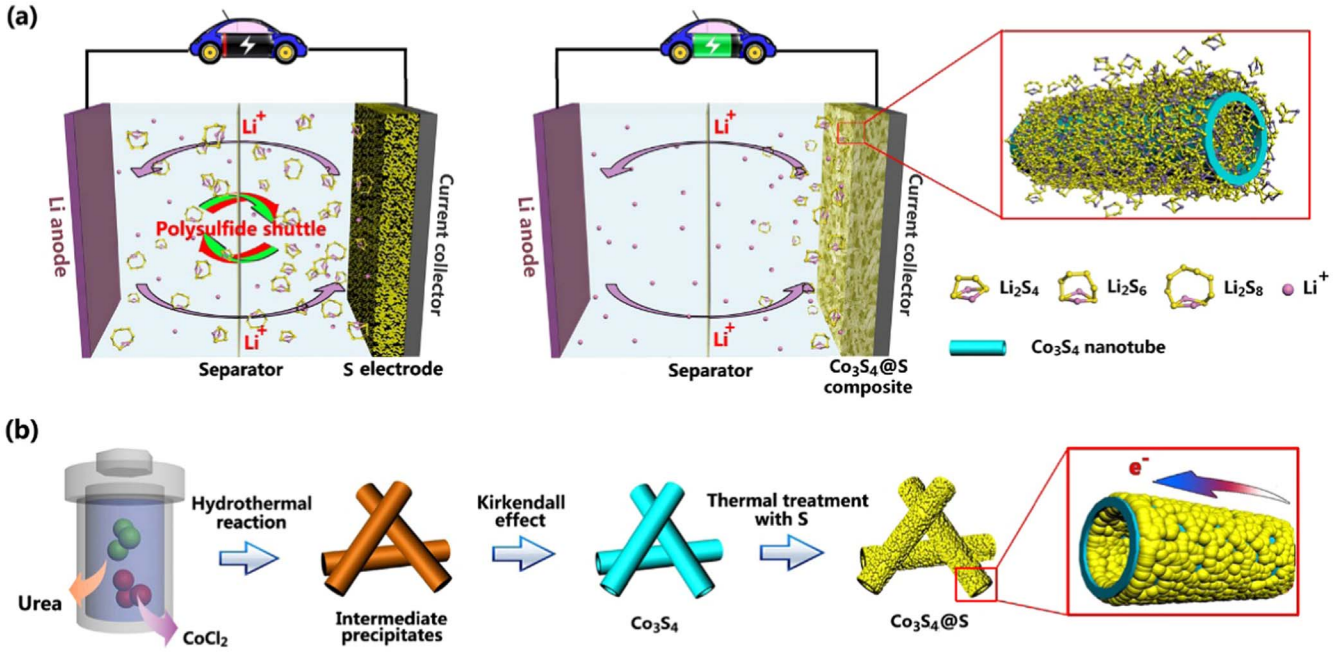

Fig. 1. Schematic illustration of (a) a Li-S battery with "shuttle effect" and a Co_3S_4@S nanotube composite to minimize the issues of polysulfides; (b) the fabrication procedure of Co_3S_4@S nanotubes.

X-ray (EDX) spectra were recorded on an FEI Tecnai F20 microscope at 200 kV. The amount of sulfur in the cathode was determined by a thermogravimetric analyzer (TGA, NETZSCH 209 F1 Libra) from room temperature to 600 °C in a nitrogen flow at a heating rate of 10 °C min^{-1}. N_2 adsorption measurements were performed on a Quantachrome Autosorb-IQ-2C-TCD-VP analyzer at 77 K using Barrett-Emmett-Teller (BET) calculations for surface area.

For the visualized adsorption characterization, a Li_2S_4 solution was synthesized by adding Li_2S and sulfur with a molar ratio of 1:3 in dimethyl ether (DME) under stirring according to literature [38]. The obtained solution containing about 1.4 mg mL^{-1} Li_2S_4 was used for the sulfide adsorption test. Co_3S_4 and acetylene black (AB) were added into 10.0 mL of Li_2S_4/DME solutions, respectively. The mixtures were adequately stirred for 0.5 h for adsorption test.

2.5. Electrochemical measurements

The sulfur cathodes were fabricated by slurry casting a mixture of 80 wt% active materials, 10 wt% AB, and 10 wt% polyvinylidene fluoride (PVDF) binder on Al foil. The sulfur loading was around 2–4 mg cm^{-2}. The obtained laminate was dried in vacuum at 50 °C. The Co_3S_4@S cathode was assembled with lithium into coin cells in an Ar-filled glove box. The electrolyte used was 1.0 M bis-(trifluoromethane) sulfonimide lithium (LiTFSI) and 0.1 M $LiNO_3$ with the 1:1 vol ratio of 1,3-dioxolane (DOL) and DME. About 40 μL electrolyte was added for each coin cell. Galvanostatic charge/discharge was carried out between 1.6 and 2.6 V using a Land Battery Tester. Cyclic voltammograms (CVs) were measured by a VSP potentiostat (Bio-Logic Corp).

For symmetrical cells, the electrodes used contain no elemental sulfur. AB or Co_3S_4 were dispersed together with PVDF in N-methyl pyrrolidone (NMP) with a weight ratio of 8:2. The slurry was cast on Al foil and dried in vacuum at 50 °C. The obtained laminates were used as the identical working and counter electrodes. The electrolyte contained about 0.5 M Li_2S_6 which was prepared by adding Li_2S and S (1:5) into the solution. CV measurements of these symmetrical cells were conducted between −0.5 and 0.5 V at a scan rate of 50 mV s^{-1}. The EIS measurements were carried out at the open circuit potential between 100 kHz and 0.01 Hz. The chronoamperometry curves were measured by the pulsed potentials between −0.5 V (60 s) and 0.5 V (60 s).

3. Results and discussion

The fabrication procedure is illustrated in Fig. 1b. The hydrothermal treatment of an aqueous urea and $CoCl_2$ solution leads to the intermediate precipitates with the nano-needle morphology. Fig. 2a and b show that the nano-needles diameter is about 80–90 nm. The XRD pattern in Fig. 2g identifies them as $Co(CO_3)_{0.35}Cl_{0.20}(OH)_{1.10}$ (JCPDS card no. 38–547). After a second hydrothermal treatment with thioacetamide (Fig. 1b), the nano-needles are converted to nanotubes due to the Kirkendall effect. The SEM images clearly indicate the hollow structures in Fig. 2c. The HRTEM image in Fig. 2d shows that the nanotube has about 15 nm thick wall and the lattice fringe of 0.55 nm, which is in agreement with the (111) plane spacing of Co_3S_4. The EDX spectrum exhibits the element distribution of Co and S along the nanotube diameter. The XRD pattern in Fig. 2g further confirms the formation of Co_3S_4 (JCPDS card no. 42–1448). The obtained Co_3S_4 nanotubes are mixed with sulfur powder. After heat treatment at 155 °C, sulfur is adsorbed to the surface of Co_3S_4 nanotubes as shown in Fig. 2e. The TEM image and EDX mapping (Fig. 2f) indicate the inclusion of sulfur into the Co_3S_4 nanotubes. The sulfur loading could be controlled by varying the sulfur/Co_3S_4 mass ratios during the heat treatment. The mass ratio of 2:1, 3:1, and 4:1 are denoted as Co_3S_4-S2, Co_3S_4-S3, and Co_3S_4-S4, respectively. The areal loading for these three samples is around 2 mg cm^{-2}. The TGA plots in Fig. 2h indicate that Co_3S_4-S2, Co_3S_4-S3, and Co_3S_4-S4 have the elemental sulfur of 66.4, 74.2, and 79.3 wt%, respectively. Their XRD patterns (Fig. 2g) show the typical combination of elemental sulfur and Co_3S_4.

The interactions between Co_3S_4 and polysulfides (Li_2S_n, n=4, 6, 8, see in Fig. S1) are studied by the first-principle calculations based on the density functional theory (DFT). The calculation details are presented in the Supporting information (SI). The binding energy (E_b) of polysulfides on the substrate is defined as $E_b=E_{sub}+E_{ps}-E_{sub+ps}$, where E_{sub}, E_{ps}, and E_{sub+ps} represent the ground-state energies of the substrate, polysulfides, and substrate-polysulfide (Fig. 3a) [30,48]. Fig. 3b and Table S1 show that the binding energies of Li_2S_4, Li_2S_6, and Li_2S_8 on Co_3S_4 are 1.61–2.76 eV, which are higher than those on graphitic carbon (0.42–0.58 eV). The first principle calculation explains the strong adsorption between polysulfides and Co_3S_4. To further evaluate the interaction between Co_3S_4 and polysulfides, the as-synthesized Co_3S_4 nanotubes were added into a 1,2-dimethoxyethane solution containing 1.4 mg mL^{-1} Li_2S_4. In the optical photo of Fig. 3d, the original yellow-brown solution turned transparent, indicating the strong adsorption. By contrast, the solution with adding the same amount of acetylene black was still yellow-brown.

Fig. 3c presents the X-ray photoelectron spectroscopy (XPS) data of pure Co_3S_4 and the Co_3S_4/Li_2S_4 precipitates, which were separated from the adsorption experiments in Fig. 3d. The Co $2p_{3/2}$ spectrum of pure Co_3S_4 has a broad peak consisting of two components of 779.3 and 780.8 eV, which correspond to Co^{3+} and Co^{2+} [57–59]. For the Co_3S_4/Li_2S_4 precipitates, the Co $2p_{3/2}$ peak shifts towards higher binding energy and pronounced satellite indicate that the electron transfer from Li_2S_4 molecules to Co [48,49,60]. Generally, both experimental and theoretical studies indicate that Co_3S_4 has the strong affinity to Li_2S_4 and as an effective sulphific host, may minimize the diffusion issues of polysulfide ions for Li-S batteries [61–63].

The electrochemical properties of Co_3S_4@S nanotube composites were characterized with lithium as the counter electrode in coin cells. Fig. 4a shows that the galvanostatic charge/discharge curves of Co_3S_4-S3 have two plateaus. The first upper voltage plateau around 2.3 V in the discharge curves is the typical characteristic of the reduction of elemental sulfur to long-order polysulfides [30,31]. The second plateau at about 2.1 V is due to the reduction of long-order polysulfides to insoluble Li_2S_2 or Li_2S [64]. The charging plateau around 2.2 V is attributed to the oxidation of Li_2S and Li_2S_2 phase to Li_2S_x (x > 2). The second charging plateau at 2.35–2.4 V represents the oxidation from polysulfides to sulfur [65]. Co_3S_4-S3 in the first cycle delivers a specific capacity of 1158 mA h g−1 AS (0.25 C) with a Coulombic efficiency of 96.0%, which gradually increases to 100% in next 10 cycles. To determine what capacity Co_3S_4 could provide, a cell with Co_3S_4 as the cathode is characterized in Fig. S2, which shows that Co_3S_4 has nearly no capacity between 1.9 and 2.6 V. Its specific capacity (< 80 mA h g^{-1}) below 1.9 V is almost negligible as compared to that of sulfur.

It is well known that Co_3S_4 has a particularly high conductivity [54], which may help to decrease the resistance of electron conduction and transfer. By contrast to the widely-used AB conductive agent, Co_3S_4 has the good affinity to polysulfides, yielding the close contact between polysulfides and conduction pathway. The good conductivity and affinity to polysulfides facilitate the electron conduction and transfer. Previous theoretic and experimental studies have demonstrated that the nanotube morphology is conducive to the formation of electron conduction network and able to significantly lower the percolation threshold [66–69]. The uniform coating or coverage of sulfur on Co_3S_4 nanotubes also reduces the ion transport length and promotes the utilization of sulfur. Thus, the Co_3S_4@S nanotube composites may have a higher capacity than the sulfur electrode.

Fig. 4b presents the charge/discharge curves of the sulfur electrode, which delivers an initial capacity of 1032 mA h g−1 AS at 0.1 C. Its Coulombic efficiency is 89.1% in the first cycle. A rapid capacity decay occurs in next few cycles. The polarization (ΔE) of Co_3S_4-S3 at a half capacity is around 0.18 V, which is lower than that of sulfur (0.22 V).

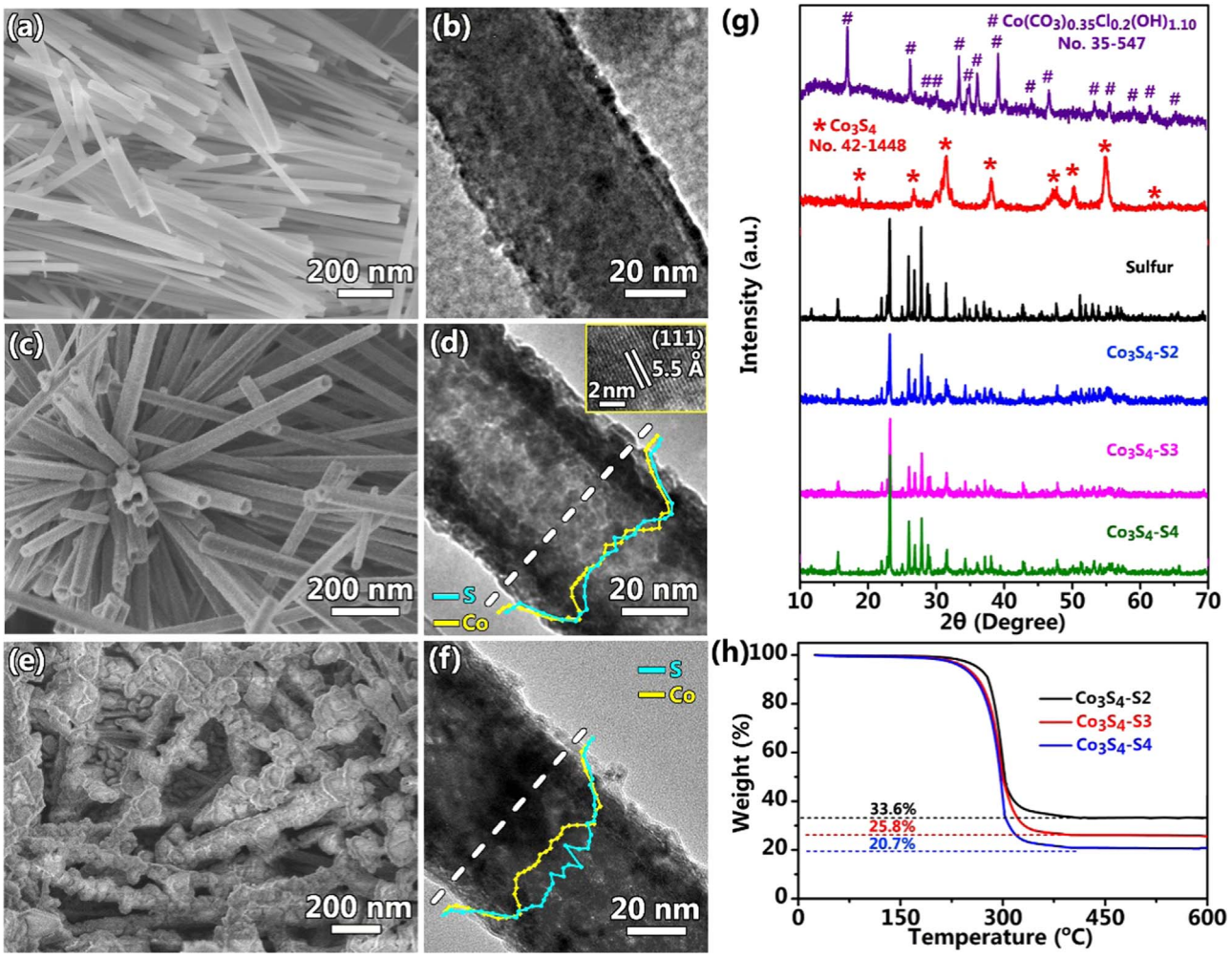

Fig. 2. SEM and TEM images of (a–b) $Co(CO_3)_{0.35}Cl_{0.20}(OH)_{1.10}$ intermediate precipitates, (c–d) Co_3S_4 nanotubes, and (e–f) Co_3S_4/sulfur composite (Co_3S_4-S3). The inset in (d) is the HRTEM image of Co_3S_4 nanotube walls. The plots in (d–f) are EDX element Co and S distribution along the diameters of Co_3S_4. (g) XRD patterns of intermediate precipitates, Co_3S_4, elemental sulfur, and Co_3S_4@S composite. (h) TGA curves of three Co_3S_4@S samples.

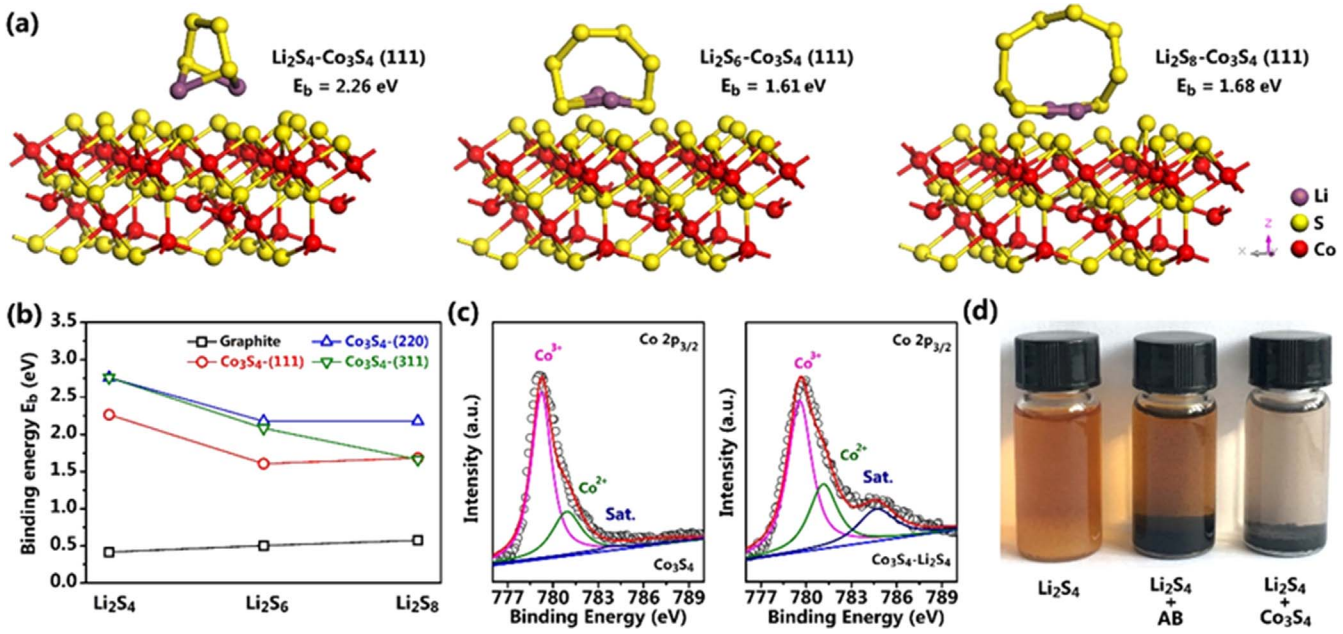

Fig. 3. (a) Typical binding geometries and energies of three polysulfide molecules (Li_2S_4, Li_2S_6, Li_2S_8) on Co_3S_4 (111) surface. (b) Binding energies of polysulfides anchored on different Co_3S_4 surfaces. (c) High-resolution XPS spectra of Co $2p_{3/2}$ of the pristine Co_3S_4 and the Co_3S_4 powder separated from the adsorption test. (d) Optical photo of Li_2S_4 adsorption on AB and pristine Co_3S_4.

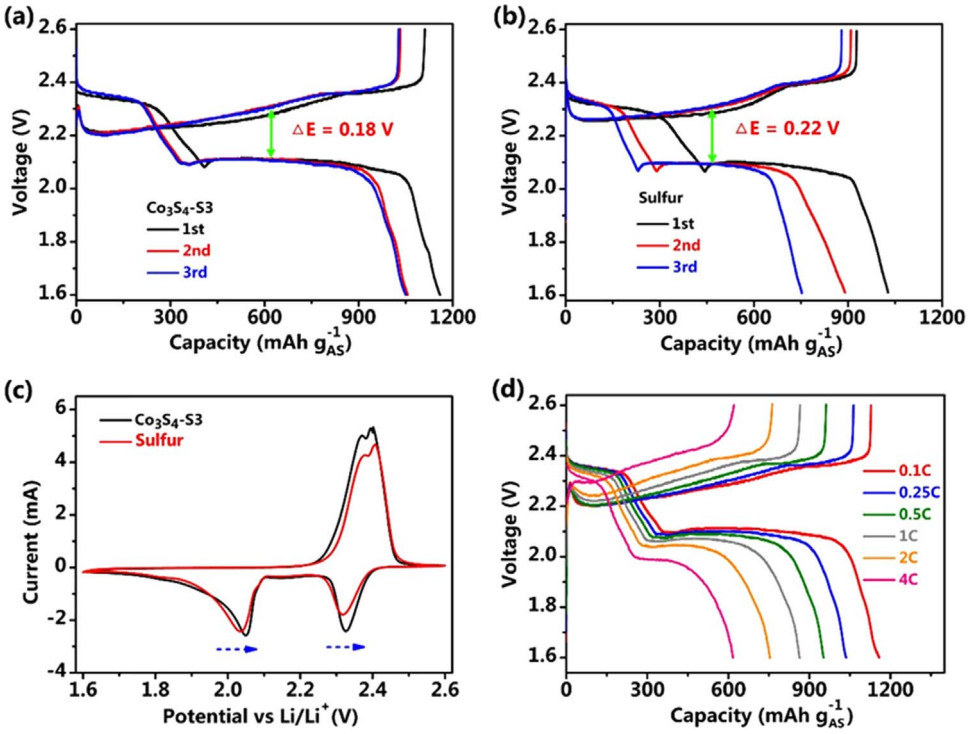

Fig. 4. Charge/discharge curves of (a) Co_3S_4-S3 and (b) sulfur electrodes. (c) CV curves of Co_3S_4-S3 and sulfur electrodes. (d) Charge/discharge curves of Co_3S_4-S3 at varied C rates (S loadings: 2 mg cm^{-2}).

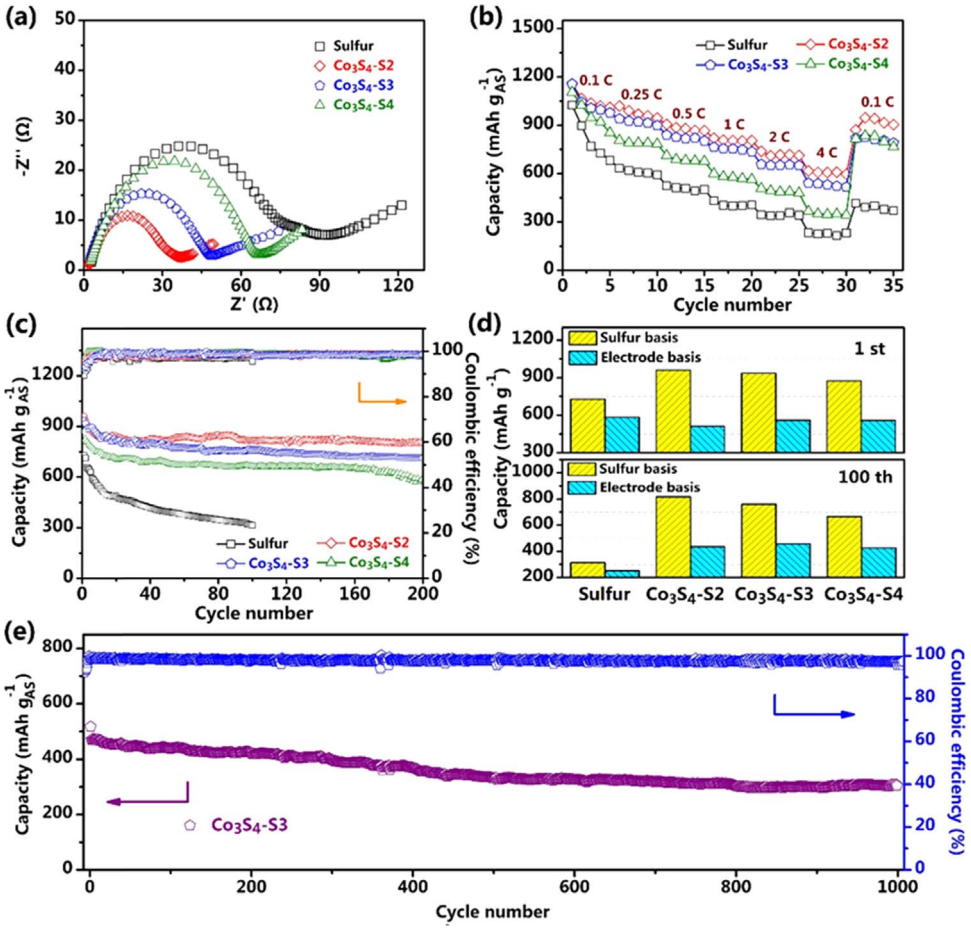

Fig. 5. (a) Nyquist plots of sulfur and Co_3S_4@S nanotube electrodes at open circuit voltage. (b) Rate capability and (c) cycling properties (0.5 C) of sulfur and Co_3S_4@S electrodes. (d) The capacity comparison of different samples on different bases. (e) Cycling properties of the Co_3S_4-S3 electrode at 5 C.

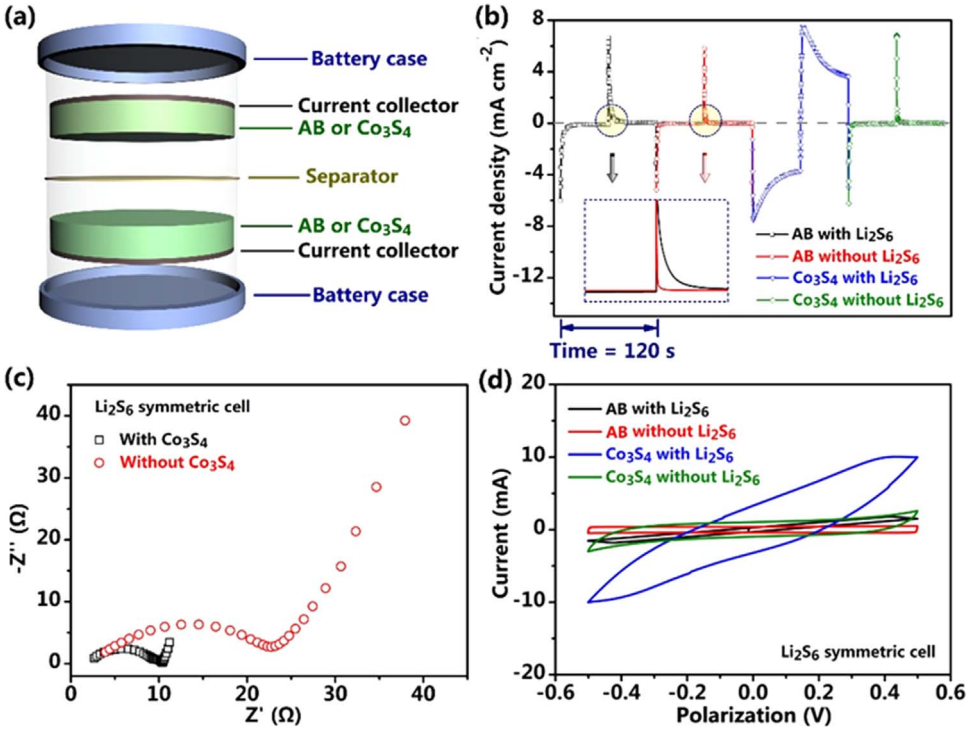

Fig. 6. (a) Schematic illustration of a symmetric cell. (b) Chronoamperometric curves, (c) EIS spectra, and (d) CV curves of the Li_2S_6 and AB symmetrical cells.

Fig. S3 presents the polarization over potentials of sulfur and three Co_3S_4@S nanotube composites at 0.25 and 0.5 C. The polarization ΔE of all four electrodes increases with C rates. Among them, the sulfur electrode shows the largest polarization at each C rate.

Fig. 4c shows the CV curves of the Co_3S_4-S3 composite and sulfur electrodes at a scan rate of 0.1 mV s^{-1} between 1.6 and 2.6 V. The reducing branches of both CV curves exhibit two typical peaks, which correspond to the multi-step lithiation of sulfur [70]. The oxidizing branches show two partly overlapping peaks around 2.4 V [71]. It is clearly seen that as compared to the sulfur electrode, the redox peaks for Co_3S_4-S3 shift towards the quasi-equilibrium potentials, indicating of relatively fast electrochemical reactions [72].

It agrees with the plateau gap difference between charge/discharge curves in Fig. 4a and b. Fig. 4d shows the charge/discharge properties of the Co_3S_4-S3 electrode at varied rates. The specific capacity decreases from 1267 to 617 mA h g−1 AS when the C rate increases from 0.05 to 4 C. Even at 4 C, the two typical plateaus still appear except some voltage drops due to the kinetic resistances [73–75].

Fig. 5a shows the electrochemical impedance spectroscopy (EIS) results of the sulfur and Co_3S_4@S electrodes. The Nyquist plots of the four electrodes basically consist of the typical semicircles and linear tails. As shown in Fig. 5a and Table S2, the high-frequency intercepts range from 2 to 2.9 Ω. Among them, Co_3S_4-S2 has the lowest contact resistance. The semicircle diameter in the medium-frequency range is proportional to the charge transfer resistance. Fig. 5a shows that Co_3S_4-S2 only has a half charge transfer resistance of the sulfur electrode. The EIS results imply that there are more complicated mechanisms for fast kinetics besides the facilitated electron conduction caused by the good conductivity of Co_3S_4 nanotubes.

Fig. 5b shows the rate capabilities of the sulfur and Co_3S_4@S electrodes. Their specific capacities generally decrease with the increase of C rates. At 0.1 C, the sulfur and Co_3S_4@S electrodes deliver a specific capacity of ~1100 mA g−1 AS, which indicates the similar utilization ratio of sulfur materials at low C rates. When the cycling rates increase to 4 C, the deliverable capacities decrease to 605, 540 and 347 mA h g−1 AS for Co_3S_4-S2, Co_3S_4-S3, and Co_3S_4-S4, respectively. By contrast, the sulfur electrode could only retain a capacity of ~239 mA h g−1 AS at 4 C. These results indicate the good rate capability of Co_3S_4@S composites. More importantly, when the C rate returns to 0.1 C, the Co_3S_4@S nanotube electrodes are able to recover more deliverable capacities than the sulfur electrode. The large capacity gap at 0.1 C is observed between the cycled Co_3S_4@S composites and sulfur electrodes. The specific capacities of the four electrodes do not return to the initial values of 0.1 C. There are more irreversible processes inside the sulfur electrode than the Co_3S_4@S composites. These irreversible processes may reduce the long term cycling stability of the sulfur electrode without Co_3S_4. During the galvanostatic cycling, the sulfur and Co_3S_4@S nanotube electrodes show relatively high initial capacities at 0.5 C and slight capacity decays in the first 10 cycles as shown in Fig. 5c. Their Coulombic efficiencies gradually increase to ~100% in the first 10 cycles. After 20 cycles, the Co_3S_4@S composites deliver relatively stable capacities. In contrast, the sulfur electrode still exhibits the obvious capacity decay.

The battery characterization requires the studies on the materials, electrode, cell, and battery levels [76]. The specific capacity based on the sulfur mass partly reveals the utilization ratio of active sulfur. It does not include the mass of conductive agents and binders. For a practical sulfur cathode, the electrode-based capacity is usually important to compare the real performance of different electrode configurations. Fig. 5d summarizes the specific capacities of the four electrodes at the initial and 100th cycles on active sulfur and total electrode bases (the electrode basis includes the mass of active sulfur, Co_3S_4 nanotubes, conductives agents, and binders), respectively. It can be seen that Co_3S_4 nanotubes are able to concurrently improve the electrode-based capacity and cyclability.

The long-term cycling performance in Fig. 5e demonstrates that the Co_3S_4-S3 composite has a superior cyclability with an initial capacity of 517 mA h g−1 AS at 5 C and a low capacity fading rate of 0.041% per cycle. After 1000 cycles, it remains a specific capacity of 305 mA h g−1 AS, which corresponds to 59% of its initial value. When the areal loading of sulfur increases to ~4 mg cm^{-2}, the Co_3S_4-S3 composite also exhibits high capacity and cyclability as shown in Fig. S4. The good cyclability may be attributed to the Co_3S_4 nanotubes because they are able to effectively conduct electrons and adsorb polysulfides.

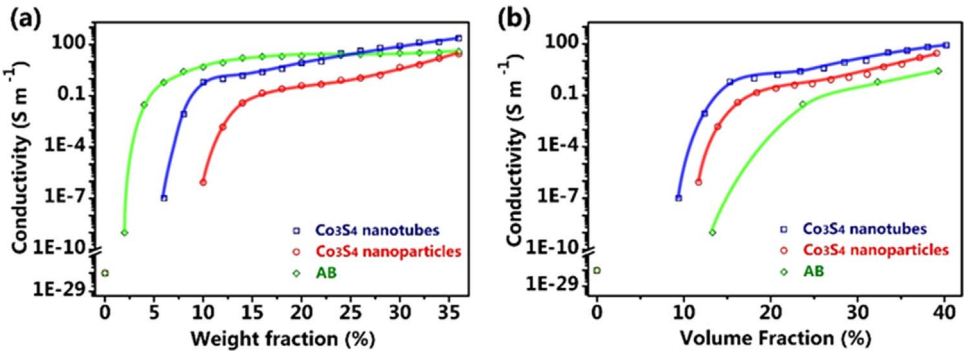

Fig. 7. Electric conductivity of sulfur composite films containing Co_3S_4 nanotubes, nanoparticles, or AB with respect to (a) mass and (b) volume fractions.

Meanwhile, the high affinity of sulfur species to Co_3S_4 enables uniform distribution on the inner and outer surface of Co_3S_4 nanotubes. The uniform coating decreases kinetic resistances of Li-ion diffusion and improves the cycling properties of Co_3S_4@S composite electrodes. Table S3 shows the comparison of performance with other polar materials in Li-S batteries.

The polysulfides adsorption is proportional to the surface area of Co_3S_4 nanotubes. The BET measurements reveal that Co_3S_4 nanotubes have only a surface area of 31 m^2 g^{-1} (Fig. S5), which is not enough to adsorb all sulfur species. To explore what factors further enhance the electrochemical properties of Co_3S_4@S nanotube electrodes, a symmetric cell (Fig. 6a) using Co_3S_4 nanotube electrodes is constructed with or without adding Li_2S_6 in the electrolyte, respectively. Fig. 6b presents the chronoamperometry curves of Co_3S_4 and AB symmetrical cells. With adding Li_2S_6 in the electrolyte, both the Co_3S_4 and AB cells shows much higher current response than cells without Li_2S_6. It implies that the lithiation/delithiation reactions dominate the current responses instead of double-layer capacitance. The EIS spectra in Fig. 6c show that the reaction semicircle of the Co_3S_4 cell has a much smaller diameter than that of the AB cell. According to Zhang and Li's reports [48,72,77], the reduced charge transfer resistance (R_{ct}) of symmetric Co_3S_4 cell represents the enhanced electrode reaction kinetics [78]. Similarly, the CV curves in Fig. 6d show that the Co_3S_4 cell has the high current responses as compared to the AB cell in Li_2S_6-containing electrolyte. It indicates that Co_3S_4 not only absorbs sulfur species, but also accelerates the electrochemical conversion of polysulfides [48,72]. The results obtained from the symmetric cells lead us to conclude that the Co_3S_4 nanotubes enhance the kinetics of the lithiation/delithiation reaction of polysulfides. In conjunction with the polysulfide affinity and conductivity enhancement of Co_3S_4, the catalytic effect further explains why the Co_3S_4 nanotubes electrodes have the high specific capacity and good rate and cycling properties.

Both the polysulfide adsorption and catalytic kinetic enhancement are related to the surface area of Co_3S_4. To improve the electrochemical properties of sulfur cathodes, nanostructuring Co_3S_4 is an easy approach to obtaining the high surface area. However, nanostructured Co_3S_4 may have the varied morphologies which influence the electron conductivity of sulfur/Co_3S_4 composite cathodes. It is well known that the conductivity of composite electrodes can be described by $\sigma = \sigma_{ca} \bullet (f - f_c)^{\tau}$, where σ_{ca} is the conductivity of conductive agents (Co_3S_4 or AB), τ is the critical exponent for conductivity, f is the ratio of conductive agents, and f_c is the percolation threshold [79]. Fig. 7a and b show that Co_3S_4 nanotubes have the relatively lower percolation threshold than Co_3S_4 nanoparticles (Fig. S6) on the bases of either weight or volume fractions because the large aspect ratio of nanotubes readily forms a conducting network (as shown in Fig. S7). Fig. 7a shows that AB has the lowest percolation threshold on the weight basis. However, AB requires the higher volume fraction to form the percolation network because of its particulate morphology and much lower density than Co_3S_4 as shown in Fig. 7b. In view of the high catalytic capability of Co_3S_4 and low density of AB, it is suggested that the combination of Co_3S_4 nanotubes and AB may serve to enhance the electrochemical properties of sulfur composite cathodes as illustrated in Fig. S8.

The overall performance of Li-S batteries is sensitive to the ratio of sulfur to inactive components. High S loading is always desired for practical applications. As for three issues which Li-S batteries face (S insulator, shuttle effects, and volume changes), the concepts of using hollow hosts, catalysis, conductive agents, and adsorbents have been proposed to address each issue respectively in previous reports [23,49,80,81]. Our tentative study shows that it is advantageous to combine these approaches into one structure of Co_3S_4 nanotubes, which realized the S ratio of 79.3 wt% and the S loading of up to 4 mg cm^{-2}. The approach of making multifunctional nanotube catalysts with the conducting and absorbing capabilities provides more opportunities to further improve the high-performance Li-S batteries.

4. Conclusions

We have proposed the use of multifunctional Co_3S_4 nanotubes as sulfur host with a high sulfur loading and good electrochemical properties. Due to the high electron conductivity and polysulfide affinity of Co_3S_4, the specific capacity and rate capabilities of Co_3S_4@S nanotube electrodes are significantly improved. The high affinity between Co_3S_4 and polysulfides minimize the polysulfide ions dissolution and increase the cyclability of the sulfur composite electrodes. In addition, Co_3S_4 nanotubes can also enhance the redox kinetics of polysulfides. More importantly, the multifunctional nanotubes help to form effective conductive networks. An optimized Co_3S_4@S nanotube electrode is able to deliver a capacity of 1267 mA h g–1 AS at 0.05 C and show a low capacity decay rate of 0.041% per cycle at 5 C. Even after 1000 cycles, it still remains a specific capacity of 305 mA h g–1 AS. Generally, we demonstrate a multifunctional Co_3S_4@S nanotubes composite which enables a Li-S battery with high capacity, good rate capabilities, and cycling properties.

Acknowledgements

This work is supported by the Thousand Youth Talents Plan (No. 128010), Jiangsu Outstanding Youth Funds (BK20160012), “Jiangsu Shuangchuang” Program, and Nantong Fundamental Research Funds (GY12016040). The numerical calculations in this paper have been done on the computing facilities in the High Performance Computing Center (HPCC) of Nanjing University.

Appendix A. Supporting information

Supplementary data associated with this article can be found in the online version at doi:10.1016/j.nanoen.2017.05.009.

References

[1] A. Manthiram, S.H. Chung, C.X. Zu, Adv. Mater. 27 (2015) 1980–2006.
[2] Q. Pang, X. Liang, C.Y. Kwok, L.F. Nazar, Nat. Energy 1 (2016) 16132.
[3] Y.S. Su, Y.Z. Fu, T. Cochell, A. Manthiram, Nat. Commun. 4 (2013) 2985.
[4] J.Q. Huang, Q. Zhang, F. Wei, Energy Storage Mater. 1 (2015) 127–145.
[5] J. Liang, Z.H. Sun, F. Li, H.M. Cheng, Energy Storage Mater. 2 (2016) 76–106.
[6] Z.W. Seh, Y.M. Sun, Q.F. Zhang, Y. Cui, Chem. Soc. Rev. 45 (2016) 5605–5634.
[7] C. Huang, J. Xiao, Y.Y. Shao, J.M. Zheng, W.D. Bennett, D.P. Lu, L.V. Saraf, M. Engelhard, L.W. Ji, J.G. Zhang, X.L. Li, G.L. Graff, J. Liu, Nat. Commun. 5 (2014) 3015.
[8] Y. Zhao, W.L. Wu, J.X. Li, Z.C. Xu, L.H. Guan, Adv. Mater. 26 (2014) 5113–5118.
[9] Y.V. Mikhaylik, J.R. Akridge, J. Electrochem. Soc. 151 (2004) A1969–A1976.
[10] W. Ni, J.L. Cheng, X.D. Li, Q. Guan, G.X. Qu, Z.Y. Wang, B. Wang, RSC Adv. 6 (2016) 9320–9327.
[11] M.R. Wang, H.Z. Zhang, W. Zhou, X.F. Yang, X.F. Li, H.M. Zhang, J. Mater. Chem. A 4 (2016) 1653–1662.
[12] W. Chen, Z.A. Zhang, Q. Li, Y.Q. Lai, J. Li, ChemElectroChem 2 (2015) 246–252.
[13] S. Xiao, S.H. Liu, J.Q. Zhang, Y. Wang, J. Power Sources 293 (2015) 119–126.
[14] H. Kim, H.D. Lim, J. Kim, K. Kang, J. Mater. Chem. A 2 (2014) 33–47.
[15] S. Evers, L.F. Nazar, Acc. Chem. Res. 46 (2013) 1135–1143.
[16] Y. Yang, G.Y. Zheng, Y. Cui, Chem. Soc. Rev. 42 (2013) 3018–3032.
[17] N. Moreno, M. Agostini, A. Caballero, J. Morales, J. Hassoun, Chem. Commun. 51 (2015) 14540–14542.
[18] F. Wu, J. Li, Y.F. Tian, Y.F. Su, J. Wang, W. Yang, N. Li, S. Chen, L.Y. Bao, Sci. Rep. 5 (2015) 13340.
[19] G. He, S. Evers, X. Liang, M. Cuisinier, A. Garsuch, L.F. Nazar, ACS Nano 7 (2013) 10920–10930.
[20] Y.H. Qu, Z.A. Zhang, X.W. Wang, Y.Q. Lai, Y.X. Liu, J. Li, J. Mater. Chem. A 1 (2013) 14306–14310.
[21] Y.C. Qiu, G.L. Rong, J. Yang, G.Z. Li, S. Ma, X.L. Wang, Z.H. Pan, Y. Hou, M.N. Liu, F.M. Ye, W.F. Li, Z.W. Seh, X.Y. Tao, H.B. Yao, N. Liu, R.F. Zhang, G.M. Zhou, J.P. Wang, S.S. Fan, Y. Cui, Y.G. Zhang, Adv. Energy Mater. 5 (2015) 1501369.
[22] M. Wei, P.L. Yuan, W.H. Chen, J.H. Hu, J. Mao, G.S. Shao, Electrochim. Acta 178 (2015) 564–570.
[23] C. Tang, B.Q. Li, Q. Zhang, L. Zhu, H.F. Wang, J.L. Shi, F. Wei, Adv. Funct. Mater. 26 (2016) 577–585.
[24] J.H. Yan, X.B. Liu, X.F. Wang, B.Y. Li, J. Mater. Chem. A 3 (2015) 10127–10133.
[25] Z. Yuan, H.J. Peng, J.Q. Huang, X.Y. Liu, D.W. Wang, X.B. Cheng, Q. Zhang, Adv. Funct. Mater. 24 (2014) 6105–6112.
[26] K. Mi, Y. Jiang, J.K. Feng, Y.T. Qian, S.L. Xiong, Adv. Funct. Mater. 26 (2016) 1571–1579.
[27] S.H. Chung, P. Han, R. Singhal, V. Kalra, A. Manthiram, Adv. Energy Mater. 5 (2015) 1500738.
[28] Y.S. Su, Y.Z. Fu, A. Manthiram, Phys. Chem. Chem. Phys. 14 (2012) 14495–14499.
[29] C. Wu, L.X. Yuan, Z. Li, Z.Q. Yi, Y.R. Li, R. Zeng, W. Zhang, Y.H. Huang, RSC Adv. 5 (2015) 14196–14201.
[30] Q. Pang, D.P. Kundu, M. Cuisinier, L.F. Nazar, Nat. Commun. 5 (2014) 4759.
[31] S.S. Zhang, J. Power Sources 231 (2013) 153–162.
[32] Z. Deng, Z. Zhang, Y. Lai, J. Liu, J. Li, Y.J. Liu, J. Electrochem. Soc. 160 (2013) A553–A558.
[33] M. Barghamadi, A. Kapoor, C.E. Wen, J. Electrochem. Soc. 160 (2013) A1256–A1263.
[34] S.G. Zhang, K. Ueno, K. Dokko, M. Watanabe, Adv. Energy Mater. 5 (2015) 1500117.
[35] C.B. Jin, W.K. Zhang, Z.Z. Zhuang, J.G. Wang, H. Huang, Y.P. Gan, Y. Xia, C. Liang, J. Zhang, X.Y. Tao, J. Mater. Chem. A 5 (2017) 632–640.
[36] Q. Fan, W. Liu, Z. Weng, Y.M. Sun, H.L. Wang, J. Am. Chem. Soc. 137 (2015) 12946–12953.
[37] G.Y. Xu, J.R. Yuan, X.Y. Tao, B. Ding, H. Dou, X.H. Yan, Y. Xiao, X.G. Zhang, Nano Res. 8 (2015) 3066–3074.
[38] X. Liang, C. Hart, Q. Pang, A. Garsuch, T. Weiss, L.F. Nazar, Nat. Commun. 6 (2015) 5682.
[39] X.Y. Tao, J.G. Wang, Z.G. Ying, Q.X. Cai, G.Y. Zheng, Y.P. Gan, H. Huang, Y. Xia, C. Liang, W.K. Zhang, Y. Cui, Nano Lett. 14 (2014) 5288–5294.
[40] X.Y. Tao, J.G. Wang, C. Liu, H.T. Wang, H.B. Yao, G.Y. Zheng, Z.W. She, Q.X. Cai, W.Y. Li, G.M. Zhou, C.X. Zu, Y. Cui, Nat. Commun. 7 (2016) 11203.
[41] S.C. Han, H.S. Kim, Y.M. Kang, H.J. Ahn, H.J. Ahn, Batteries and supercapacitors, San Francisco, 2003.
[42] J. Liang, L.C. Yin, X.N. Tang, H.C. Yang, W.S. Yan, L. Song, H.M. Cheng, F. Li, ACS Appl. Mater. Interfaces 8 (2016) 25193–25201.
[43] H.A. Salem, G. Babu, C.V. Rao, L.M.R. Arava, J. Am. Chem. Soc. 137 (2015) 11542–11545.
[44] N. Ding, L. Zhou, C.W. Zhou, D.S. Geng, J. Yang, S.W. Chien, Z.L. Liu, M.F. Ng, A.S. Yu, T.S.A. Hor, M.B. Sullivan, Y. Zong, Sci. Rep. 6 (2016) 33154.
[45] H.J. Peng, T.Z. Hou, Q. Zhang, J.Q. Huang, X.B. Cheng, M.Q. Guo, Z. Yuan, L.Y. He, F. Wei, Adv. Mater. Interfaces 1 (2014) 1400227.
[46] H.J. Peng, Z.W. Zhang, J.Q. Huang, G. Zhang, J. Xie, W.T. Xu, J.L. Shi, X. Chen, X.B. Cheng, Q. Zhang, Adv. Mater. 28 (2016) 9551–9558.
[47] J. Liu, B. Chen, Y. Kou, Z. Liu, X. Chen, Y.B. Li, Y.D. Deng, X.P. Han, W.B. Hu, C. Zhong, J. Mater. Chem. A 4 (2016) 11060–11068.
[48] Z. Yuan, H.J. Peng, T.Z. Hou, J.Q. Huang, C.M. Chen, D.W. Wang, X.B. Cheng, F. Wei, Q. Zhang, Nano Lett. 16 (2016) 519–527.
[49] Q. Pang, D. Kundu, L.F. Nazar, Mater. Horiz. 3 (2016) 130–136.
[50] J. Zhou, N. Lin, W.L. Cai, C. Guo, K.L. Zhang, J.B. Zhou, Y.C. Zhu, Y.T. Qian, Electrochim. Acta 218 (2016) 243–245.
[51] Z.L. Ma, Z. Li, K. Hu, D.D. Liu, J. Huo, S.Y. Wang, J. Power Sources 325 (2016) 71–78.
[52] Y.O. Chen, Y.A. Chang, Metall. Mater. Trans. B 9 (1978) 61–67.
[53] S. Yomo, J. Magn. Magn. Mater. 31–34 (1983) 331–332.
[54] R.J. Bouchard, P.A. Russo, A. Wold, Inorg. Chem. 5 (1965) 685–688.
[55] M. Jana, S. Saha, P. Samanta, N.C. Murmu1, N.H. Kim, T. Kuila, J.H. Lee, Nanotechnology 26 (2015) 075402.
[56] H. Behret, H. Binder, G. Sandstede, Electrochim. Acta 20 (1975) 111–117.
[57] Z.H. Wang, L. Pan, H.B. Hu, S.P. Zhao, CrystEngComm 12 (2010) 1899–1904.
[58] Z.P. Li, W.Y. Li, H.T. Xue, W.P. Kang, X. Yang, M.L. Sun, Y.B. Tang, C.S. Lee, RSC Adv. 4 (2014) 37180–37186.
[59] J. Yang, H.W. Liu, W.N. Martens, R.L. Frost, J. Phys. Chem. C 114 (2010) 111–119.
[60] G. Zhou, H. Tian, Y. Jin, X. Tao, B. Liu, R. Zhang, Z.W. Seh, D. Zhuo, Y. Liu, J. SUn, J. Zhao, C. Zu, D.S. Wu, Q.F. Zhang, Y. Cui, Proc. Nat. Acad. USA 114 (2017) 840–845.
[61] Q.T. Qu, T. Gao, H.Y. Zheng, Y. Wang, X.Y. Li, X.X. Li, J.M. Chen, Y.Y. Han, J. Shao, H.H. Zheng, Adv. Mater. Interface 2 (2015) 1500048.
[62] X.W. Wang, T. Gao, X.L. Fan, F.D. Han, Y.Q. Wu, Z.A. Zhang, J. Li, C.S. Wang, Adv. Funct. Mater. 26 (2016) 7164–7169.
[63] W.Z. Bao, D.W. Su, W.X. Zhang, X. Guo, G.X. Wang, Adv. Funct. Mater. 26 (2016) 8746–8756.
[64] P.G. Bruce, S.A. Freunberger, L.J. Hardwick, J.M. Tarascon, Nat. Mater. 11 (2012) 19–29.
[65] H.B. Yao, G.Y. Zheng, P.C. Hsu, D.S. Kong, J.J. Cha, W.Y. Li, Z.W. Seh, M.T. McDowell, K. Yan, Z. Liang, V.K. Narasimhan, Y. Cui, Nat. Commun. 5 (2014) 3943.
[66] P.C. Ma, M.Y. Liu, H. Zhang, S.Q. Wang, R. Wang, K. Wang, Y.K. Wong, B.Z. Tang, S.H. Hong, K.W. Paik, J.K. Kim, ACS Appl. Mater. Interfaces 5 (2009) 1090.
[67] W. Bauhofer, J.Z. Kovacs, Compos. Sci. Technol. 69 (2009) 1486–1498.
[68] Y.P. Liu, X.Y. He, D. Hanlon, A. Harvey, U. Khan, Y.G. Li, J.N. Coleman, ACS Nano 10 (2016) 5980–5990.
[69] G. Cunningham, M. Lotya, N. McEvoy, G.S. Duesberg, P. Schoot, J.N. Coleman, Nanoscale 4 (2012) 6260–6264.
[70] X.Q. Zhao, M. Liu, Y. Chen, B. Hou, N. Zhang, B.B. Chen, N. Yang, K. Chen, J.L. Li, L.A. An, J. Mater. Chem. A 3 (2015) 7870–7876.
[71] C. Zhang, D.H. Liu, W. Lv, D.W. Wang, W. Wei, G.M. Zhou, S.G. Wang, F. Li, B.H. Li, F.Y. Kang, Q.H. Yang, Nanoscale 7 (2015) 5592–5597.
[72] H.J. Peng, G. Zhang, X. Chen, Z.W. Zhang, W.T. Xu, J.Q. Huang, Q. Zhang, Angew. Chem. Int. Ed. 55 (2016) 12990–12995.
[73] J.X. Song, M.L. Gordin, T. Xu, S.R. Chen, Z.X. Yu, H.S. Sohn, J. Lu, Y. Ren, Y.H. Duan, D.H. Wang, Angew. Chem. Int. Ed. 54 (2015) 4325–4329.
[74] W.Y. Li, Q.F. Zhang, G.Y. Zheng, Z.W. Seh, H.B. Yao, Y. Cui, Nano Lett. 13 (2013) 5534–5540.
[75] L.C. Zeng, Y. Jiang, J. Xu, M. Wang, W.H. Li, Y. Yu, Nanoscale 7 (2015) 10940–10949.
[76] K.G. Gallagher, S.E. Trask, C. Bauer, T. Woehrle, S.F. Lux, M. Tschech, P. Lamp, B.J. Polzin, S. Ha, B. Long, Q.L. Wu, W.Q. Lu, D.W. Dees, A.N. Jansena, J. Electrochem. Soc. 163 (2016) A138–A149.
[77] R.P. Fang, S.Y. Zhao, S.F. Pei, Y.X. Cheng, P.X. Hou, M. Liu, H.M. Cheng, C. Liu, F. Li, Carbon 109 (2016) 719–726.
[78] S.S. Zhang, J. Electrochem. Soc. 159 (2012) A920–A923.
[79] L. Chang, K. Friedrich, L. Ye, P. Toro, J. Mater. Sci. 44 (2009) 4003–4012.
[80] K.Y. Xie, Y.Z. Han, W.F. Wei, H.R. Yu, C.B. Zhang, J.G. Wang, W. Lu, B.Q. Wei, RSC Adv. 5 (2015) 77348–77353.
[81] S. Rehman, T.Y. Tang, Z. Ali, X.X. Huang, Y.L. Hou, Small 13 (2017) 1700087.